

A low-loss and medium dielectric permittivity SrTiO₃/HIPS composite for rapid prototyping of next-generation microwave devices

Athanasios Goulas^{a,*}, Tsz Yan Chow^b, Tom Whittaker^b, Ian M. Reaney^c, Bala Vaidhyanathan^a, Will Whittow^b, Daniel S. Engström^b

^a Department of Materials, Loughborough University, Loughborough LE11 3TU, United Kingdom

^b Wolfson School of Mechanical, Electrical and Manufacturing Engineering, Loughborough University, LE11 3TU, United Kingdom

^c Department of Materials Science and Engineering, University of Sheffield, Sheffield S1 3JD, United Kingdom

ARTICLE INFO

Keywords:

Additive manufacturing
3D printing
Fused filament fabrication
Polymer ceramic composites
Antennas

ABSTRACT

Composite polymer/ceramic filaments for material extrusion-based fused filament fabrication (FFF) additive manufacturing, using strontium titanium oxide (SrTiO₃) ceramic fillers and high impact polystyrene (HIPS) thermoplastics were produced and their dielectric and physical properties characterised for the first time. Relative permittivity (ϵ_r), quality factor ($Q \times f$) and dielectric loss ($\tan\delta$) were measured as a function of ceramic solids loading (vol%) at 5 GHz. $\epsilon_r = 4.6$, $Q \times f = 38,378$ GHz and dielectric loss $\tan\delta = 0.001$ were obtained for a SrTiO₃/HIPS ceramic polymer composite, with 15 vol% (46 wt%) solids loading. A Plackett–Burman design of experiments was used to optimize the printing process of the ST/HIPS composites. The results of this optimisation helped achieve 3D printed parts with near-full density (99%) and $\epsilon_r = 5.3$, $\tan\delta = 0.001$. The composite materials exhibit reduced dielectric losses compared with commercially available feedstocks for FFF that are currently used for functional prototyping in the radiofrequency and telecommunications industry.

1. Introduction

There is an ongoing quest for new materials with performance that could satisfy future needs for electronic devices used in wireless and mobile communication systems operating at 5 G (3.5 – 7 GHz), 6 G (7 – 15 GHz) and (24 – 71 GHz) microwave (MW) frequencies [1]. Medium to low relative permittivity is typically required accompanied by low dielectric loss/high quality factor, a temperature coefficient of the resonant frequency close to zero and a high thermal conductivity [2–4]. Dielectric ceramics are often used in situations where $Q \times f$ is paramount but temperature stable compositions with low ϵ_r are rare [4,5], notoriously difficult to form into complex net shapes and their processing requires densification at high temperature (>1000 °C), resulting in a considerable carbon footprint.

Fused filament fabrication (FFF) is an additive manufacturing material extrusion process (ISO/ASTM 52903–1:2020) which enables shaping of 3D parts using thermoplastics. Ceramic-infilled thermoplastics (composites) are an attractive option in telecommunications since their ϵ_r can be tailored and they can still be processed to near net-shape at low temperature [6]. Polymers that are typically used in FFF are ABS,

PLA, and ASA. They can achieve $2.6 \leq \epsilon_r \leq 12$ (Table 1) when infilled with high ϵ_r ceramics such as perovskites and titanates, enabling miniaturisation with respect to metal/air designs, but often suffer from high $\tan\delta$ (0.027 – 0.003, Table 1) [7–11]. Despite such limitations, FFF has seen notable growth in recent years, since it is an accessible and low-cost technique, capable of producing either functional prototypes or low-volume production passive electronic components. Table 1 summarises the reported research on composite dielectric materials for FFF 3D printing to date.

This paper presents a novel ceramic/polymer composite material feedstock, suitable for FFF 3D printing, composed of a high-impact polystyrene matrix ($\epsilon_r \approx 2.3$) with strontium titanate ($\epsilon_r \approx 300$) ceramic particles as the filler; materials that both exhibit low dielectric loss at MW frequencies which is quintessential when synthesising low dielectric loss composites. The physical and microwave dielectric properties are measured as a function of vol% solids loading. To mitigate against any process defects, a Design of Experiments (DoE) approach was employed to optimise printing parameters and manufacture test samples of the highest solids loading composite prepared in this study. Results showcase a novel composite filament material for FFF 3D

* Corresponding author.

E-mail address: a.goulas@lboro.ac.uk (A. Goulas).

<https://doi.org/10.1016/j.addma.2024.104390>

Received 24 January 2024; Received in revised form 16 July 2024; Accepted 26 August 2024

Available online 30 August 2024

2214-8604/© 2024 The Author(s). Published by Elsevier B.V. This is an open access article under the CC BY license (<http://creativecommons.org/licenses/by/4.0/>).

printing that exhibits the lowest dielectric loss documented in the literature to-date, suitable for the fabrication of functional prototypes or small batch production of passive devices.

2. Materials and methods

2.1. Materials

High-purity (99.9 %) strontium titanium oxide SrTiO₃ (ST) ceramic powder (Merck KGaA, Darmstadt, Germany) was used with a particle size $d_{90} < 5 \mu\text{m}$. Uncoloured pellets of High-Impact Polystyrene (HIPS) thermoplastic were utilised (3DXTECH, Michigan, USA) with a nominal density of $1.04 \text{ g}\cdot\text{cm}^{-3}$.

2.2. Composite filament manufacture

HIPS pellets were mixed together with acetone in a 1:1.8 wt ratio and left to dissolve over a period of 72 hours while being continuously stirred with the aid of a magnetic stirrer. Various volume fractions of ST particles were then dispersed in the HIPS/acetone to form slurries without visible sedimentation. Prior to blending, ST particles were coated with a 2 wt% ammonium polyacrylate dispersant (Darvan 821 A, Vanderbilt Minerals Co., Gouverneur, USA) in 2-propanol, using planetary ball milling for 24 hours at 100 rpm (PM100, Retsch GmbH, Haan, Germany). The slurries were placed in a container which was sealed, immersed in an ultrasonic bath and sonicated for 30 minutes to break up any particle agglomerates. The resultant composites were poured into PTFE moulds and left to dry in ambient conditions overnight. Once dried, composites were pelletised, further dried in an oven at 80 °C for 48 hours and formed into 1.75 mm filaments using an extruder (Noztek Pro, Shoreham-by-Sea, Sussex, United Kingdom) operating at 190 °C and 60 rpm extrusion speed.

2.3. Additive manufacturing

All manufacturing experiments were conducted using a multi-process additive manufacturing system (Hydra 16 A, Hyrel3D, Norcross, GA, USA) equipped with a filament extrusion module (MK1-250, Hyrel3D, Norcross, GA, USA) and a brass nozzle with a diameter of 0.55 mm. Test samples measuring $35 \times 35 \text{ mm} \times 1 \text{ mm}$ used for characterisation of the prepared composites, were printed on a smooth borosilicate glass surface heated at 110 °C. The printing parameters included a print speed of $40 \text{ mm}\cdot\text{s}^{-1}$, a layer thickness of 0.1 mm, an extrusion width of 0.5 mm; introducing a 10 % overlap and a constant positive displacement value of 80 pulses per microlitre. A rectilinear infill pattern with alternating $-90/+90$ degrees was used. The test samples were first modelled using CAD, and the G-code for printing was generated using Hyrel3D's inbuilt slicing software (Repetrel, V4.2.565, Hyrel3D, Norcross, GA, USA).

2.4. Characterisation methods

The phase and purity of the purchased SrTiO₃ powder together with any potential interactions between the polymer matrix and the ceramic powder filler, were investigated using X-Ray diffraction (D2 Phaser

Diffraction, Bruker AXS, Karlsruhe, Germany) using CuK α radiation at $\lambda = 1.54 \text{ \AA}$, operating at 30 kV and 10 mA with a 1 mm divergence, 3 mm air-scatter and 2.5° Soller slits. Diffraction patterns were collected from $10 - 80^\circ 2\theta$, using a 0.02° step size and 15 min^{-1} sample rotation. Collected data were analysed using Bruker's proprietary software (DIFFRAC.EVA 5.2, Bruker AXS, Karlsruhe, Germany).

The particle size distribution of the ST powder was confirmed using a combination of dynamic light scattering (DLS) (Zetasizer Ultra, Mastersizer, Malvern, UK) and field-emission scanning electron microscopy (FESEM) (JSM 7100 F, JEOL Ltd., Tokyo, Japan). To prevent charging during FESEM, powder samples were sputter coated with a 80:20 wt% gold/palladium for 90 s at 25 mA (Quorum Q150T, Quorum, Edwards, Hastings, UK).

The apparent (ρ_{measured}) and relative density (ρ_{relative}) of the 3D printed test samples were measured following the Archimedes principle (ASTM D792-20), using an analytical balance (ME200, Mettler Toledo) and as a reference the theoretical density ($\rho_{\text{theoretical}}$) of the composites. Results are reported as an average of three different 3D printed samples, together with their standard deviation.

The microstructure of the composite filaments and the 3D printed test samples were examined using SEM (TM3030, Hitachi High Energy Technologies), operated in back-scattered electron mode, using an acceleration voltage of 15 kV and a working distance of 8 mm. Composite filament and 3D printed test samples, were manually snapped and mounted directly onto 12.5 mm aluminium pin stubs using conductive carbon adhesive tabs (Leit, Agar Scientific Ltd., Stansted, Essex, UK). To prevent charging during SEM, samples were sputter coated with a gold/palladium alloy in an 80:20 wt% ratio, for 90 s at 25 mA (Quorum Q150T, Quorum, Edwards, Hastings, UK).

ϵ_r , $\tan\delta$ and $Q \times f$ of additively manufactured ST/HIPS samples were determined by placing the rectangular 3D printed test samples of $35 \times 35 \text{ mm}$ and 1 mm thickness, into a split post dielectric resonator (SPDR) operating at the $f_0 = 5.1 \text{ GHz}$ (QWED, Warsaw, Poland), representative of 5 and sub-6 G systems. The properties were calculated using QWED's proprietary software. Results are reported as an average after measuring three different 3D printed samples together with the standard deviation.

2.5. Parameter development through design of experiments (DoE) methodology

A Plackett-Burman design methodology was employed to systematically investigate the impact of printing process parameters of the 3D printed test samples by using statistical software (RStudio, 2021.09.1, RStudio Team, PBC, Boston, MA). The DoE procedure was carried out only for the composite bearing the highest achieved solids loading of 15 vol%. Each of the factors was varied at two levels, with a total of 12 randomised experiments being conducted. Each experiment comprised of three replicates. Table 2 lists the chosen factors, along with their lower and upper levels. The build platform temperature of 110°C and the rectilinear infill pattern were set as fixed parameters. The analysed data were fed to a response surface single-objective optimisation algorithm, in order to obtain an optimal combination of printing process parameters that would result in fully dense samples and consequently the highest ϵ_r .

Table 1

Summary table of ceramic/polymer composites for FFF additive manufacturing reported in the literature.

Ceramic Filler	Polymer Matrix	ϵ_r	$Q \times f \text{ (GHz)}$	$\tan\delta$	Measurement Frequency (GHz)	Reference
CNT	Acrylonitrile butadiene styrene	7.5	-	-	0.01	[7]
TiO ₂	Cyclo-olefin polymer	12.35	-	0.003	16	[8]
BaTiO ₃	Acrylonitrile butadiene styrene	13	-	0.0289	15	[9]
BaTiO ₃	Acrylonitrile butadiene styrene	2.6 – 8.7	-	0.005 – 0.027	15	[10]
Ba _{0.77} Sr _{0.23} TiO ₃	Acrylonitrile butadiene styrene	6.05	10,433	0.007	5	[11]
SrTiO ₃	High-impact polystyrene	5.3	38,378	0.001	5	This work

Table 2
Factors and levels used for the Puckett-Burman design.

Factors	Lower Level	Upper Level
Printing speed (mm·s ⁻¹)	25	50
Layer height (mm)	0.1	0.3
Extrusion width (mm)	0.4	0.55
Extrusion temperature (°C)	230	250
Pulses per microliter	60	80

3. Results and discussion

3.1. Raw materials characterisation

Fig. 1 shows the room-temperature X-ray diffraction patterns of as-received (AR) ST powder. The diffraction peaks from the ST powder are indexed to the cubic perovskite SrTiO₃ with Pm3̄m (221) group and lattice parameter, $a = 0.39 \text{ \AA}$ (ICDD PDF 00-035-0734). The theoretical density of the ST phase was calculated from the XRD data at $\rho_{ST} = 5.1 \text{ g}\cdot\text{cm}^{-3}$. Results from particle size analysis, revealed a unimodal particle size distribution, Fig. 2a, with a mean particle size, $d_{mean} = 3.97 \text{ \mu m}$ and polydispersity index (PI) = 0.2342. This was confirmed from SEM images, Fig. 2b.

3.2. Dielectric and physical properties of additively manufactured ST/HIPS composites

Fig. 3 presents the dielectric properties of the 3D printed test samples at 5 GHz as a function of ST solids loading (vol%), using the printing process parameters listed in Section 2.3. ϵ_r increased progressively from 2.3 ± 0.02 for the unfilled test samples, up to 4.6 ± 0.08 for the samples loaded with 15 vol% ceramic particles. This increase is ascribed to the higher ϵ_r of ST. However, the $\tan\delta$ increased as a function of the solids loading accompanied by a reduction in $Q \times f$. The dielectric losses of the unfilled samples were measured with $\tan\delta = 0.0006 \pm 0.00002$ and $Q \times f = 55,546 \pm 150 \text{ GHz}$, while the samples that contained 15 vol% ST, achieved $\tan\delta = 0.001 \pm 0.00006$ and $Q \times f = 38,378 \pm 112 \text{ GHz}$. We note that ST/HIPS composite filaments with solids loading past that of 15 vol%, exhibited an extremely brittle behaviour and were not further

assessed.

Dielectric loss in ceramic/polymer composites is related to factors such as: a) material impurities, b) the filler being inherently more lossy than the matrix material and c) the formation of interfaces between the two dissimilar materials, introducing anharmonicity in the vibrational phonon modes. Nonetheless, the 3D printed ceramic/polymer composites presented in this study, exhibited lower loss than commercially available materials [12] and two orders of magnitude less than laminates such as FR4 ($\epsilon_r = 4.9 \pm 0.001$; $\tan\delta = 0.014 \pm 0.0001$ and $Q \times f = 973 \pm 6 \text{ GHz}$ at 5 GHz). No issues with the layer-to-layer adhesion or delamination were evident, while printing with the composite materials.

Fig. 4a is a comparison of the theoretical density of the ST/HIPS composites and the measured density of the 3D printed test samples, as a function of the ST solids loading (vol%). A difference of up to $\delta\rho = 11 \%$, between the measured and theoretical density values was observed due to: a) the effect of the increased volume fraction of the ceramic particles present in the composite, that may reduce the flow characteristics of the composite [13], b) randomly occurring bubbles/air voids in the composite filament, a product from the outgassing of remaining solvent; shown in Fig. 5, and c) a combination of air gaps between the printed layers and small pores between the adjacent printed filaments that form a monolayer. The addition of ST particles was found to change the morphology of the polymer matrix when the filler content reached 10 vol% or higher. High magnification electron images in Fig. 5 show that the polymer's morphology transitioned to a cellular-like structure. This change may be due to the interaction between the filler and the polymer.

Porosity is known to decrease the microwave properties of the 3D printed samples, as air inclusions with $\epsilon_{air} \approx 1$, reduce the effective ϵ_r [13,14]. Additionally, entrapment of moisture within those air inclusions, may negatively influence the dielectric loss [15]. Fig. 4b overlays measured ($\epsilon_r^{measured}$) and corrected for porosity ($\epsilon_r^{corrected}$), values at 5 GHz. The latter depicts material performance excluding porosity. 3D printed test samples with the maximum solids loading achieved in this study, exhibited a $\epsilon_r^{corrected} = 5.3$ taking into account 11 % porosity. $\epsilon_r^{corrected}$ values are necessary to describe the performance of the composite material, regardless of the chosen fabrication process. Table 3 summarises the physical and dielectric properties of the

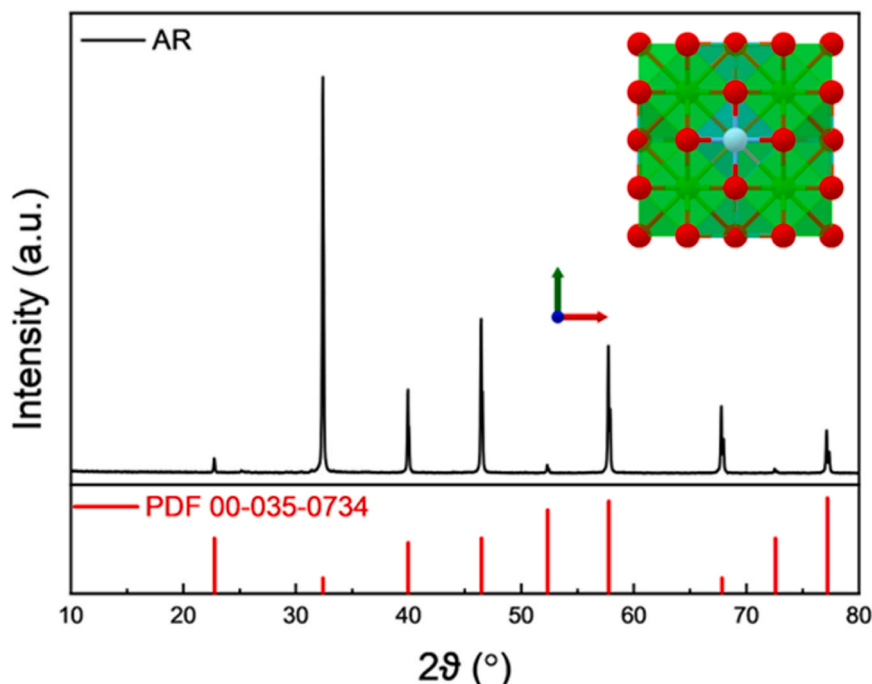


Fig. 1. RT-XRD patterns of the as-received (AR) SrTiO₃ powder.

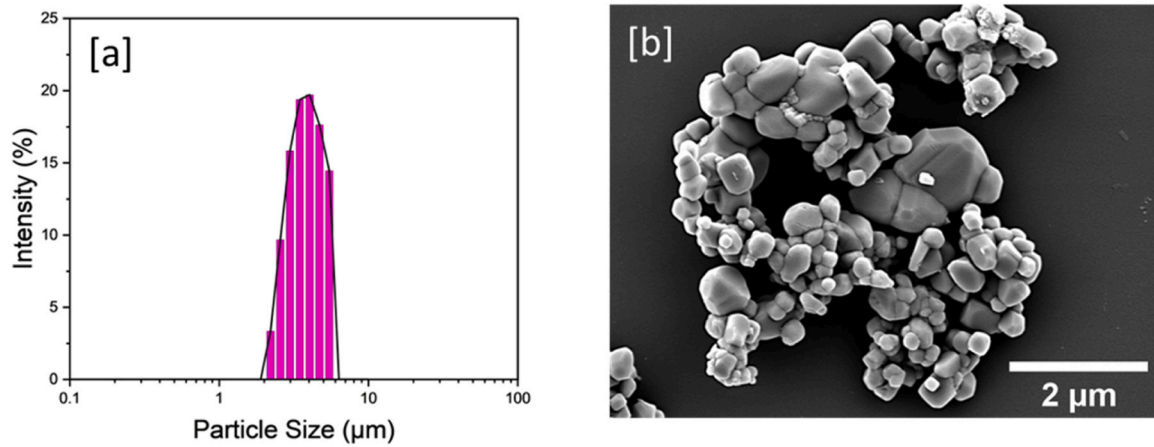


Fig. 2. [a] Particle size distribution and [b] scanning electron micrograph of the ST powder.

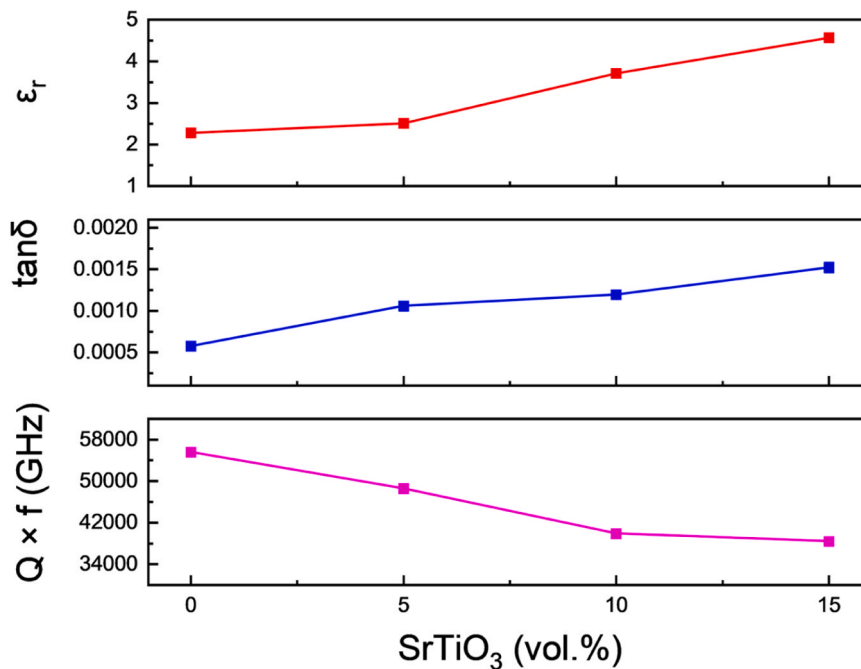


Fig. 3. Relative permittivity (ϵ_r), dielectric loss ($\tan\delta$), and quality factor ($Q \times f$) vs. ST/HIPS volume fraction of the 3D printed test samples, measured at 5 GHz using the SPDR.

3D printed test samples.

Fig. 6a shows the RT-XRD patterns of the ST/HIPS composite test samples as a function of ST solids loading. The diffraction pattern collected from the non-filled HIPS polymer matrix, exhibited a single broad peak (commonly known as a halo) at low diffraction 2θ angles, which is characteristic for amorphous polymers, such as HIPS. The diffraction patterns for the ceramic/polymer samples bearing 5 – 15 vol %, contained reflections indexed to the SrTiO₃ cubic perovskite crystalline phase (ICDD PDF 00–035–0734). With increasing volume fraction of the infilling ceramic particles, the amorphous low-angle halo disappeared into the background. XRD results suggest that the constituents of the ceramic/polymer composite remain heterogeneous.

Fig. 6b is an overlay of the DSC curves, from the ST/HIPS composite test samples, heated between RT to 500°C, as a function of their solids loading. All DSC plots showed a series of minor endotherm peaks in the temperature range of $T_1 = 25 - 60$ °C, ascribed to the evaporation of adsorbed moisture or remaining solvents and one major endotherm at approximately $T_2 = 430$ °C, associated with the decomposition of HIPS.

All values are in close agreement with the known thermophysical properties of the individual constituent materials within the composite [16,17]. Thermal conductivity and thermal decomposition of the composite were affected by the increasing volume fraction of ST. Both weight-corrected heat flow and the latent heat of fusion reduced as the vol% fraction of ST increased due to the inherent difference in the CTE between ST and HIPS which causes localised concentration of stress at the interface between the ceramic particles and the polymer matrix [18]. This stress concentration creates thermal barriers that eventually may reduce the transfer of heat. Moreover, the introduction of ceramic particles in a polymer matrix is expected to cause scattering of phonons at the interface between the two materials [19]. With an increasing number of ceramic particles in each composite, the interfacial surface contact area is also expected to increase, thereby slowing down the flow of phonons due to scattering and thus reducing the overall conductivity.

Fig. 7 shows a comparison of the ϵ_r measurements of the additively manufactured test samples as a function of the ST solids loading (φ) with the theoretical values (ϵ_r^{eff}), estimated via the effective medium theory

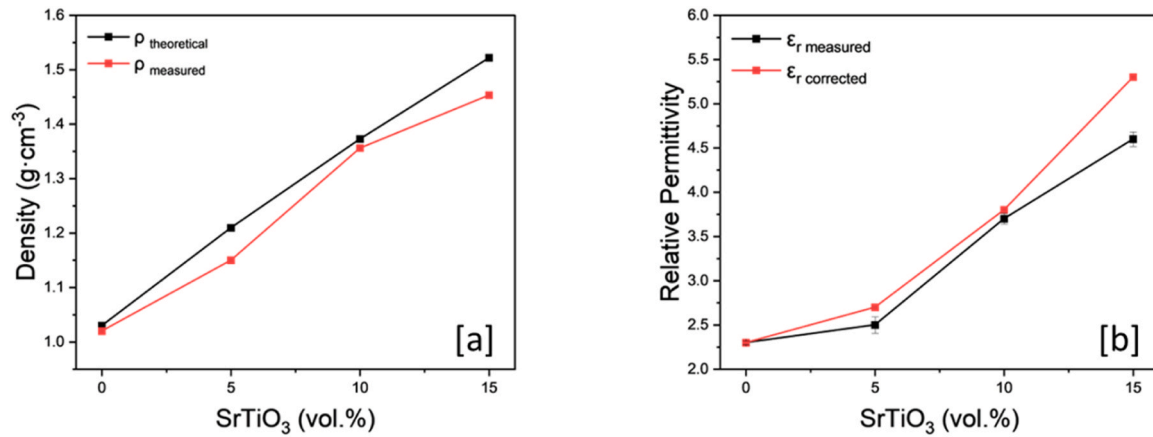


Fig. 4. [a] Theoretical and measured density of the 3D printed samples as a function of ST solids loading (vol.) and [b] measured and corrected relative permittivity at 5 GHz.

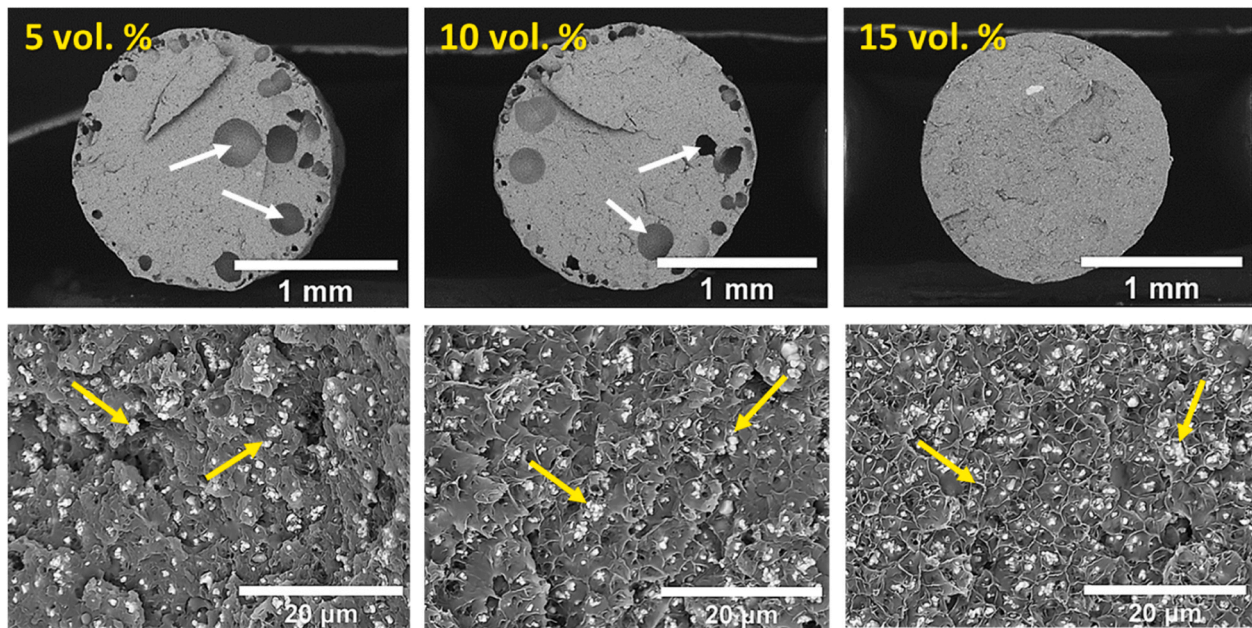


Fig. 5. Electron micrographs showing cross sections of the composite filaments (top row) and the dispersion of the ceramic particles through the HIPS matrix (bottom row), as a function of their solids loading. The white arrows denote the gas pores and the yellow arrows show the strontium titanate filler particles.

Table 3
Dielectric and physical properties of additively manufactured SrTiO₃/HIPS composites.

SrTiO ₃ (vol%)	SrTiO ₃ (wt%)	ϵ_r measured $\pm \sigma$	$\tan\delta \pm \sigma$	$Q \times f \pm \sigma$ (GHz)	ρ theoretical (g·cm ⁻³)	ρ measured $\pm \sigma$ (g·cm ⁻³)	ρ relative (%)	ϵ_r corrected
0	0	2.3 \pm 0.02	0.0006 \pm 0.00002	55546 \pm 150	1.0	1.0 \pm 0.002	99 %	2.3
5	19	2.5 \pm 0.09	0.001 \pm 0.00006	48546 \pm 766	1.2	1.1 \pm 0.009	94 %	2.7
10	34	3.7 \pm 0.06	0.001 \pm 0.00002	39874 \pm 110	1.4	1.3 \pm 0.004	98 %	3.8
15	46	4.6 \pm 0.08	0.001 \pm 0.00006	38378 \pm 112	1.5	1.4 \pm 0.010	89 %	5.3

(EMT) [20], Lichtenecker [21], Maxwell-Garnett [22], Pooh-Shin [23], and Wiener models [24] (Eq. 1 – 5) that are commonly used to predict the effective permittivity (ϵ_r effective) of two-component composites [6], that may exhibit differences in shape of the infilling particles or their distribution (uniform or non-uniform) [25]. Measured relative permittivity values of 3D printed HIPS test samples ($\epsilon_r = 2.3 \pm 0.02$) and ST pellets sintered at 1350 °C for 2 h ($\epsilon_r = 360 \pm 5.6$) were used in the models. None of the models matched the measured ϵ_r eff of the ST/HIPS composite material throughout solids loading range of 0 – 15 vol%

because the 3D printed samples were not fully dense and therefore the measurements, did not fully represent the ϵ_r of the composite. However, for ϵ_r corrected, the Lichtenecker model was in closest agreement. The latter also highlights, why 3D printed parts may not always perform as expected in terms of their dielectric properties. To mitigate against this, optimisation of the printing process is required, which is further discussed in the following section.

EMT

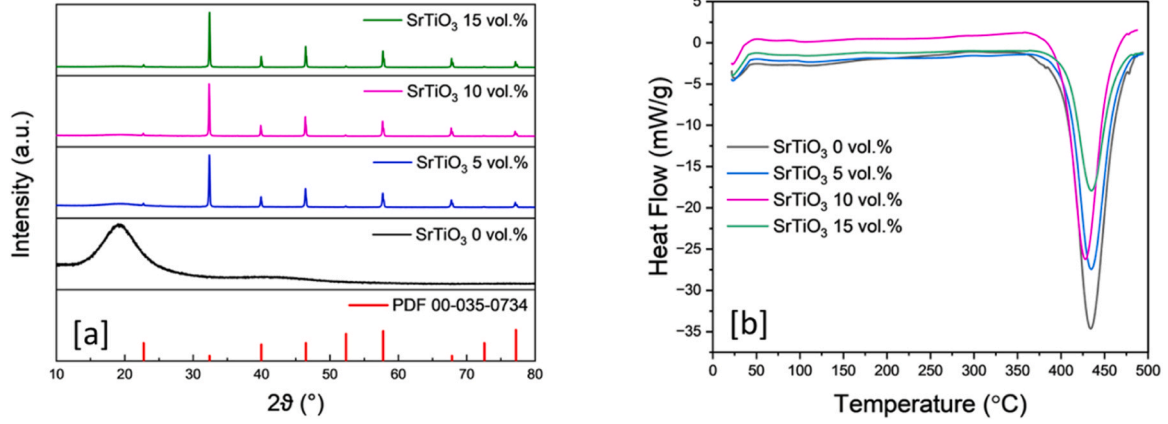


Fig. 6. [a] Diffraction patterns and [b] DSC curve overlay of 3D printed ST/HIPS composites.

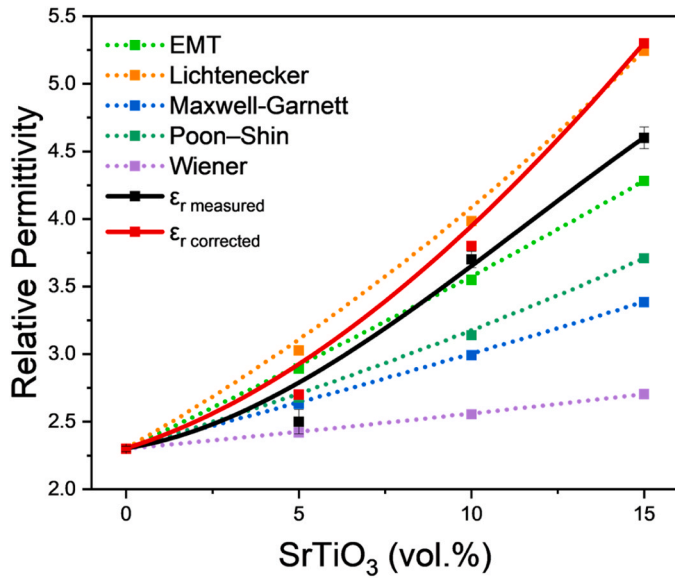


Fig. 7. Measured relative permittivity values as a function of SrTiO₃ solids loading in comparison to theoretical model.

$$\epsilon_{\text{reff}} = \epsilon_{\text{HIPS}} * \left(1 + \left(\frac{\varphi * (\epsilon_{\text{ST}} - \epsilon_{\text{HIPS}})}{\epsilon_{\text{HIPS}} + n * (1 - \varphi) * (\epsilon_{\text{ST}} - \epsilon_{\text{HIPS}})} \right) \right) \quad (1)$$

Lichtenecker

$$\ln \epsilon_{\text{eff}} = \varphi * \ln \epsilon_{\text{ST}} + (1 - \varphi) * \ln \epsilon_{\text{HIPS}} \quad (2)$$

Maxwell-Garnett

$$\frac{\epsilon_{\text{reff}} - \epsilon_{\text{HIPS}}}{\epsilon_{\text{reff}} + 2 * \epsilon_{\text{HIPS}}} = \varphi * \frac{\epsilon_{\text{ST}} - \epsilon_{\text{HIPS}}}{\epsilon_{\text{ST}} + 2 * \epsilon_{\text{HIPS}}} \quad (3)$$

Poon-Shin

$$\epsilon_{\text{reff}} = \left[1 + \frac{\varphi * \left(\frac{\epsilon_{\text{ST}}}{\epsilon_{\text{HIPS}}} - 1 \right)}{\varphi + \left(1 - \frac{\varphi}{3} \right) * \left(\frac{\epsilon_{\text{ST}}}{\epsilon_{\text{HIPS}}} \right) * (1 - \varphi) + \varphi + 2} \right] \quad (4)$$

Wiener

$$\epsilon_{\text{reff}} = \frac{\epsilon_{\text{HIPS}} * \epsilon_{\text{ST}}}{\varphi * \epsilon_{\text{ST}} + (1 - \varphi) * \epsilon_{\text{HIPS}}} \quad (5)$$

3.3. Printing process optimisation through Plackett-Burman design of experiments

The properties of parts produced via FFF are subject to the optimisation of parameters such as: layer height, printing speed, extrusion temperature and flow rate. In the case of functional prototyping for electromagnetics, density is the main physical property of interest, as it is proportional to ϵ_r which affects the performance of the designed device. In this study, Error! Reference source not found. extrusion width ($p = 0.002$) and the pulses per microlitre ($p = 0.043$) were identified as the two main factors which affected density and therefore the ϵ_r of the 3D printed test samples; shown in Table 4. Extrusion width is the distance between the two adjacent printed filaments that form a monolayer, while pulse per microlitre refers to an equipment-specific setting that controls the material flow through the hot end.

Based on the collected and analysed data for the 15 vol% ST/HIPS composites, the single-target surface response optimisation algorithm suggested that a combination of 25 mm·s⁻¹ printing speed, 0.3 mm layer thickness, 0.4 mm extrusion width, 230 °C extrusion temperature and 80 pulses per microlitre extrusion, would result in fully dense 3D printed test samples with $\epsilon_r \approx 5.3$, within a 95 % confidence interval. Fig. 8 presents electron micrographs from 3D printed and cross-sectioned 15 vol% ST/HIPS test samples, before and after process optimisation. The printed samples with optimised process parameters after the DoE procedure, measured $\epsilon_r = 5.3 \pm 0.02$ and $\tan \delta = 0.001 \pm 0.00005$, which corresponds to $\rho_{\text{measured}} = 1.49 \pm 0.01 \text{ g}\cdot\text{cm}^{-3}$ ($\rho_{\text{relative}} = 99.3 \%$).

4. Conclusions

This study investigated the manufacture and dielectric characterisation at microwave frequencies, of a novel ceramic/polymer composite to be used as feedstock for FFF 3D printing. Composite ceramic/polymer filaments of 1.75 mm in diameter, made of submillimetre strontium titanate ceramic fillers dispersed within a high-impact polystyrene polymer matrix, suitable for FFF were manufactured. A maximum solids

Table 4

ANOVA coefficient table for factorial regression of the 15 vol% 3D printed composite test samples.

Term	Effect	Coeff	SE Coef	T-Value	P-Value	VIF
Constant		3.701	0.126	29.34	0.000	
Printing Speed	-0.457	-0.229	0.126	-1.81	0.113	1.00
Extrusion width	-1.189	-0.595	0.126	-4.71	0.002	1.00
Extrusion temperature	-0.375	-0.187	0.126	-1.49	0.181	1.00
Pulses per microlitre	0.624	0.312	0.126	2.47	0.043	1.00

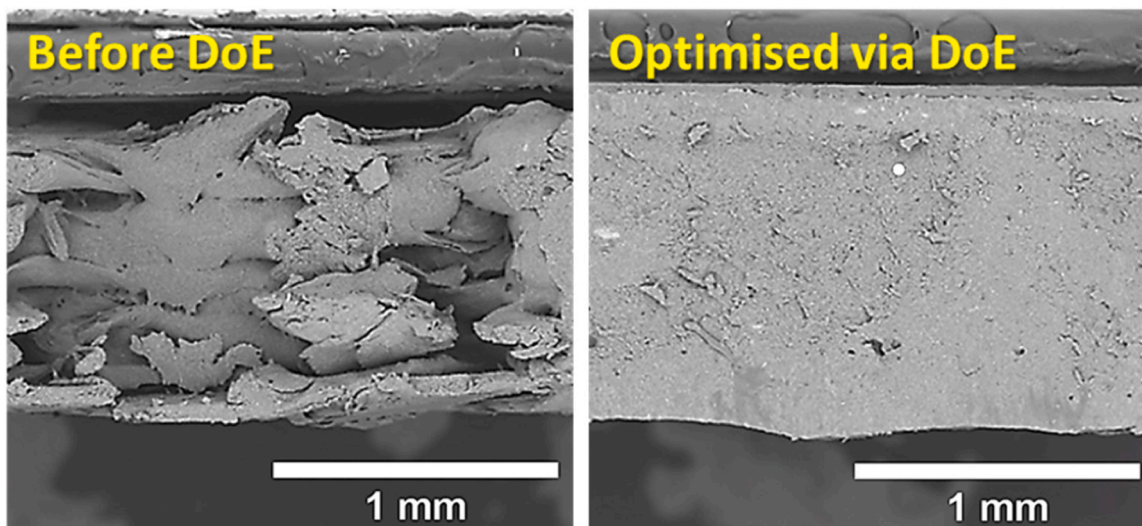


Fig. 8. ST/HIPS composite test samples' cross-sections, before and after printing optimisation via DoE.

loading of 15 vol% (46 wt%), resulted into 3D printed samples that achieved $\epsilon_r = 4.6$, $Q \times f = 38,378$ GHz and $\tan\delta = 0.001$ at 5 GHz. Printing optimisation via the Plackett-Burman design of experiments methodology, helped achieve 3D printed samples of $\epsilon_r = 5.3$, matching the theoretical properties of the 15 vol% composite. The composites exhibited lower dielectric losses, compared to similar studies previously reported in the available literature.

CRediT authorship contribution statement

Athanasios Goulas: Writing – review & editing, Writing – original draft, Visualization, Validation, Supervision, Project administration, Methodology, Investigation, Formal analysis, Data curation, Conceptualization. **Tsz Yan Chow:** Methodology, Investigation, Formal analysis, Data curation. **Tom Whittaker:** Validation, Methodology, Investigation, Formal analysis, Data curation. **Ian M. Reaney:** Writing – review & editing, Validation, Project administration, Funding acquisition. **Bala Vaidhyanathan:** Writing – review & editing, Supervision, Funding acquisition. **Will Whittow:** Writing – review & editing, Validation, Supervision, Resources, Project administration, Funding acquisition. **Daniel S. Engstrom:** Writing – review & editing, Supervision, Resources, Funding acquisition.

Declaration of Competing Interest

The authors declare that they have no known competing financial interests or personal relationships that could have appeared to influence the work reported in this paper.

Data Availability

Data will be made available on request.

Acknowledgements

This work was funded by EPSRC research grants SYMETA (EP/N010493/1) and ANISAT (EP/S030794/1). The authors acknowledge use of the facilities in the Loughborough Materials Characterisation Centre and at the Department of Chemistry at Loughborough University.

References

- [1] W. Hong, Z.H. Jiang, C. Yu, D. Hou, H. Wang, C. Guo, Y. Hu, L. Kuai, Y. Yu, Z. Jiang, Z. Chen, J. Chen, Z. Yu, J. Zhai, N. Zhang, L. Tian, F. Wu, G. Yang, Z.

- C. Hao, J.Y. Zhou, The role of millimeter-wave technologies in 5G/6G wireless communications, *IEEE J. Microw.* 1 (2021) 101–122, <https://doi.org/10.1109/JMW.2020.3035541>.
- [2] A. Raveendran, M.T. Sebastian, S. Raman, Applications of microwave materials: a review, *J. Electron Mater.* 48 (2019), <https://doi.org/10.1007/s11664-019-07049-1>.
- [3] J. Varghese, N. Joseph, H. Jantunen, S.K. Behera, H.T. Kim, M.T. Sebastian, Microwave materials for defense and aerospace applications. *Handbook of Advanced Ceramics and Composites*, Springer International Publishing, 2020, pp. 165–213, https://doi.org/10.1007/978-3-030-16347-1_9.
- [4] I.M. Reaney, D. Iddles, Microwave dielectric ceramics for resonators and filters in mobile phone networks, *J. Am. Ceram. Soc.* 89 (2006) 2063–2072, <https://doi.org/10.1111/j.1551-2916.2006.01025.X>.
- [5] W. Lou, M. Mao, K. Song, K. Xu, B. Liu, W. Li, B. Yang, Z. Qi, J. Zhao, S. Sun, H. Lin, Y. Hu, D. Zhou, D. Wang, I.M. Reaney, Low permittivity cordierite-based microwave dielectric ceramics for 5G/6G telecommunications, *J. Eur. Ceram. Soc.* 42 (2022) 2820–2826, <https://doi.org/10.1016/j.jeurceramsoc.2022.01.050>.
- [6] S.B. Basturk, C.E.J. Dancer, T. McNally, Fabrication and characterization of composites of a perovskite and polymers with high dielectric permittivity, *Mater. Res Bull.* 135 (2021), <https://doi.org/10.1016/j.materresbull.2020.111126>.
- [7] N. Vidakis, A. Maniadi, M. Petousis, M. Vamvakaki, G. Kenanakis, E. Koudoumas, Mechanical and electrical properties investigation of 3D-printed acrylonitrile-butadiene-styrene graphene and carbon nanocomposites, *J. Mater. Eng. Perform.* 29 (2020) 1909–1918, <https://doi.org/10.1007/s11665-020-04689-x>.
- [8] V. Kosamiya, J. Wang, Composite feedstock filaments for fused deposition modeling (FDM) of microwave interconnects, *IEEE Trans. Compon. Packag. Manuf. Technol.* (2023), <https://doi.org/10.1109/TCPMT.2023.3249574>.
- [9] Y. Wu, D. Isakov, P.S. Grant, Fabrication of composite filaments with high dielectric permittivity for fused deposition 3D printing, *Materials* 10 (2017), <https://doi.org/10.3390/ma10101218>.
- [10] F. Castles, D. Isakov, A. Lui, Q. Lei, C.E.J. Dancer, Y. Wang, J.M. Janurudin, S. C. Speller, C.R.M. Grovenor, P.S. Grant, Microwave dielectric characterisation of 3D-printed BaTiO₃/ABS polymer composites, *Sci. Rep.* 6 (2016) 1–8, <https://doi.org/10.1038/srep22714>.
- [11] A. Goulas, J.R. McGhee, T. Whitaker, D. Ossai, E. Mistry, W. Whittow, B. Vaidhyanathan, I.M. Reaney, J. (Yiannis), C. Vardaxoglou, D.S. Engström, Synthesis and dielectric characterisation of a low loss BaSrTiO₃/ABS ceramic/polymer composite for fused filament fabrication additive manufacturing, *Addit. Manuf.* 55 (2022) 102844, <https://doi.org/10.1016/j.addma.2022.102844>.
- [12] A. Goulas, T. Whitaker, W. Whittow, Fused filament fabrication additive manufacturing and characterisation at loughborough university for RF applications, 16th Eur. Conf. Antennas Propag. (EuCAP) (2022).
- [13] A. Goulas, S. Zhang, D.A. Cadman, J. Järveläinen, V. Mylläri, W.G. Whittow, J.Y. C. Vardaxoglou, D.S. Engström, The impact of 3D printing process parameters on the dielectric properties of high permittivity composites, *Des. (Basel)* 3 (2019), <https://doi.org/10.3390/designs3040050>.
- [14] A.H. Sihvola, J.A. Kong, Effective permittivity of dielectric mixtures, *IEEE Trans. Geosci. Remote Sens.* 26 (1988) 420–429, <https://doi.org/10.1109/36.3045>.
- [15] R. Ratheesh, M.T. Sebastian, Polymer-ceramic composites for microwave applications, *J. Microw. Mater. Appl. 2V Set.* (2017) 481–535, <https://doi.org/10.1002/9781119208549.ch11>.
- [16] Z. Katancić, J. Travaš-Sejdić, Z. Hrnjak-Murgić, Study of flammability and thermal properties of high-impact polystyrene nanocomposites, *Polym. Degrad. Stab.* 96 (2011) 2104–2111, <https://doi.org/10.1016/j.polymdegradstab.2011.09.020>.
- [17] Z. Katancić, J. Travaš-Sejdić, Z. Hrnjak-Murgić, J. Jelencić, Thermal decomposition of fire-retarded high-impact polystyrene and high-impact polystyrene/ethylene-

- vinyl acetate blend nanocomposites followed by thermal analysis, *J. Elastomers Plast.* 46 (2014) 233–252, <https://doi.org/10.1177/0095244312465301>.
- [18] C.P. Wong, R.S. Bollampally, Thermal conductivity, elastic modulus, and coefficient of thermal expansion of polymer composites filled with ceramic particles for electronic packaging, *J. Appl. Polym. Sci.* 74 (1999) 3396–3403, [https://doi.org/10.1002/\(SICI\)1097-4628\(19991227\)74:14<3396::AID-APP13>3.0.CO;2-3](https://doi.org/10.1002/(SICI)1097-4628(19991227)74:14<3396::AID-APP13>3.0.CO;2-3).
- [19] G. Alva, Y. Lin, G. Fang, Thermal and electrical characterization of polymer/ceramic composites with polyvinyl butyral matrix, *Mater. Chem. Phys.* 205 (2018) 401–415, <https://doi.org/10.1016/j.matchemphys.2017.11.046>.
- [20] C.P. Wong, T. Marinis, Jianmin Qu, Yang Rao, A precise numerical prediction of effective dielectric constant for polymer-ceramic composite based on effective-medium theory, *IEEE Trans. Compon. Packag. Technol.* 23 (2000) 680–683, <https://doi.org/10.1109/6144.888853>.
- [21] A.V. Goncharenko, V.Z. Lozovski, E.F. Venger, Lichtenecker's equation: applicability and limitations, *Opt. Commun.* 174 (2000) 19–32, [https://doi.org/10.1016/S0030-4018\(99\)00695-1](https://doi.org/10.1016/S0030-4018(99)00695-1).
- [22] V.A. Markel, Introduction to the Maxwell Garnett approximation: tutorial, *J. Opt. Soc. Am. A* 33 (2016) 1244, <https://doi.org/10.1364/josaa.33.001244>.
- [23] Y.M. Poon, F.G. Shin, A simple explicit formula for the effective dielectric constant of binary 0-3 composites, *J. Mater. Sci.* 39 (2004) 1277–1281, <https://doi.org/10.1023/B:JMSE.0000013886.21054.e4>.
- [24] K.K. Karkkainen, A.H. Sihvola, K.I. Nikoskinen, Effective permittivity of mixtures: numerical validation by the FDTD method, *IEEE Trans. Geosci. Remote Sens.* 38 (2000) 1303–1308, <https://doi.org/10.1109/36.843023>.
- [25] A. Goulas, S. Zhang, J.R. McGhee, D.A. Cadman, W.G. Whittow, J.C. Vardaxoglou, D.S. Engström, Fused filament fabrication of functionally graded polymer composites with variable relative permittivity for microwave devices, *Mater. Des.* 193 (2020) 108871, <https://doi.org/10.1016/j.matdes.2020.108871>.